Progress In Electromagnetics Research, Vol. 156, 13–24, 2016

Low-Profile On-Board Antenna with a Broad Beam Based on Three-Current Model

Ren Wang, Bing-Zhong Wang*, Changhai Hu, Cheng Gong, and Xiao Ding

Abstract—A low-profile three-current model is proposed to guide the design of an on-board antennas with a broad beam. Based on this model, an on-board three-element antenna is designed. When the side length of the ground is infinite, the 3-dB beamwidths in the xz plane and yz plane are all 180°, and the radiation pattern in the xy plane has a gain fluctuation less than 3 dB. When the side length of the ground is 2λ, the measured 3-dB beamwidths in the xz plane and yz plane are 141° and 148°, respectively. A quasi-hemispherical radiation pattern can be obtained based on the proposed three-current model.

1. INTRODUCTION

Broad coverage of antenna radiation is desired in many military and civil applications, such as communication systems and radar systems [1, 2]. Broad coverage can be obtained using two basic kinds of methods. The first one is a multi-beam array [3, 4], including wide-angle scanning arrays [5]; the second one is a broad-beam antenna with a quasi-hemispherical pattern [6–8]. For the wide-angle scanning array with a two-dimensional broad beam coverage, the pattern of each element should have a hemispherical coverage in the ideal situation. Therefore, a broad-beam antenna can be used as a single antenna and can also be applied in planar arrays to obtain a broad coverage.

In [9] and [10], crossed microstrip radiators parallel to the metal ground were used to broaden the two-dimensional beam by offsetting the narrow beamwidth in the E plane with wide beamwidth in the H plane. The broad beams of the antennas in [9] and [10] can cover up to ±60°. However, low elevation range cannot be covered with this kind of structures because antennas with electric radiators should have a small ground to realize the broad beam because of the boundary condition.

To achieve a broad beam in the condition of large ground, mixed-mode antennas have been proposed, such as combining dipole radiation modes and monopole radiation modes [11, 12]. The radiation patterns of the dipole-mode and monopole-mode can cover high and low elevation areas. Therefore, a broad beam can be obtained by optimizing the weights of the two radiation modes. With the model in [11], some broad-beam antennas and wide-angle scanning arrays were proposed [13–16]. However, the high profile of a monopole-mode radiator is a problem of this model.

For on-board applications, especially cloaking receiving systems, a high profile is undesired. Bare antennas can receive signals, but they may be detectable from the outside because they may perturb surrounding as scatterers. A proper cloak over the broad-beam antenna may allow the covered antenna to receive incident signals and simultaneously reduce the antenna's scattered radiation. Thus, the antenna will be essentially undetectable [17–19]. However, the concealable heights of existing cloak layers are limited [20–23], which require that the covered antenna has a low profile. Therefore, proposing a novel low-profile model to obtain a broad beam is significant.

Received 20 February 2016, Accepted 27 March 2016, Scheduled 26 April 2016

* Corresponding author: Bing-Zhong Wang (bzwang@uestc.edu.cn).

The authors are with the Institute of Applied Physics, University of Electronic Science and Technology of China, Chengdu 610054, China.

In this paper, firstly, a three-current model with a low profile is proposed to design the broad-beam on-board antenna. Afterward, a three-element antenna is designed based on this model. The proposed antenna with a broad beam can be used in wireless communication systems.

2. THREE-CURRENT MODEL

For on-board antennas with a large planar ground, the beamwidth on the vertical cannot be wider than 180°, and the broadest three-dimensional beam is hemispherical. To guide the design of broad-beam antennas, an ideal hemispherical pattern situation is discussed in this section. Five directions of the hemispherical pattern, ($\theta = 90°$, $\varphi = 0°$), ($\theta = 90°$, $\varphi = 90°$), ($\theta = 90°$, $\varphi = 180°$). ($\theta = 90°$, $\varphi = -90°$), and ($\theta = 0°$), should have equal amplitudes. The five-equal-direction (FED) condition is necessary but not sufficient for the hemispherical pattern. To design an antenna satisfying the FED condition, a three-current (TC) model is shown in Fig. 1. This model is composed of three currents, where the currents can be electric or magnetic currents. Current 1 (C1) and Current 3 (C3) have a spacing of d and equal amplitudes but inverse phases. The distance between Current 2 (C2) and the model centre O is d_2.

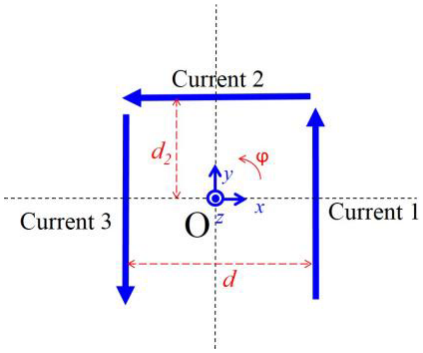

Figure 1. Three-current model to obtain a quasi-hemispherical radiation pattern.

In the TC model, the pattern nulls of C2 and the pattern maximums of the binary array (C1 and C3) both direct to ($\theta = 90°$, $\varphi = 0°$) and ($\theta = 90°$, $\varphi = 180°$); the pattern maximums of C2 and the pattern nulls of the binary array are both located at the yz plane in the directions of ($\theta = 90°$, $\varphi = \pm 90°$) and ($\theta = 0°$). Moreover, the pattern has equal amplitudes in the directions ($\theta = 90°$, $\varphi = \pm 90°$) and ($\theta = 0°$), and equal amplitudes in the directions ($\theta = 90°$, $\varphi = 0°$), and ($\theta = 90°$, $\varphi = 180°$). Therefore, the FED condition can be simplified as an equality relationship that the pattern maximum of C2 is equal to that of the binary array.

The TC model can be surveyed in the free space to determine the necessary condition to obtain a two-dimensional broad pattern because the pattern in the upper half-space will not change when the TC model with magnetic currents or electric currents is parallel to and on the surface of an infinite electric wall or magnetic wall, respectively. Taking O as the reference point of phase, the pattern factor of C2 in the yz plane and that of the binary array in the xz plane can be respectively written as [24]

$$AF_{C_2} = A_2 e^{-j(\sin\theta)2\pi d_2/\lambda} \tag{1}$$

$$AF_{binary} = 2jA_1 \sin[(\sin\theta)\pi d/\lambda] \tag{2}$$

where A_1 is the amplitude of C1 and C3, A_2 the amplitude of C2, and $j = \sqrt{-1}$. If the model satisfies the FED condition, the pattern of binary array in the direction ($\theta = 90°$, $\varphi = 0°$) and the pattern of C2 in the direction ($\theta = 90°$, $\varphi = 90°$) should have an equal amplitude, then

$$A_2 = 2A_1 \sin(\pi d/\lambda) \tag{3}$$

It is notable that this simplified condition does not include the relation between d and d_2. Because we just consider five special directions, the condition is necessary but not sufficient. Parameters of the

TC model, such as the relation between d and d_2, may have effects on the broad beam even when the FED condition is satisfied.

To determine the effect of some key parameters, such as the phase difference dp between C1 and C2, distance d between C1 and C3, and distance d_2 between C2 and the model centre O, some numerical simulations of the TC mode are discussed under the condition of Eqn. (3). The model is simulated using CST Microwave Studio. In the following discussions, three $\lambda/50$-length electric dipoles are placed on an infinite magnetic wall, and the distance between the dipoles and the magnetic wall is 0.05λ, where λ is the free-space wavelength corresponding to 2.4 GHz. The three electric dipoles, Dipole 1, Dipole 2, and Dipole 3, are corresponding to C1, C2, and C3, respectively. It is the complementary structure of three magnetic currents on an infinite electric wall.

Figure 2 shows the effect of phase difference dp between Dipole 1 and Dipole 2 on the radiation pattern at 2.4 GHz. If the 3-dB beamwidths in the xz plane, yz plane, and $\varphi = 45°/-135°$ plane are all 180°, and the 3-dB beamwidths in the xy plane is 36°, we note the case as a good broad-beam performance; if not, we note it as a poor one. The solid lines and dashed lines represent the cases of good and poor broad-beam performances, respectively. In all of the cases, the distance d_2 between Dipole 2 and the model centre is fixed at $\lambda/2$. From these figures, we can see that the 3-dB beamwidths of all the cases are 180° in the xz plane and yz plane, but not in the $\varphi = 45°/-135°$ plane. In the xz plane and yz plane, there are three equal-amplitude controlling directions. In the $\varphi = 45°/-135°$ plane, there is only one controlling direction. The limited controlling directions cause that broad beams can only be obtained when the key parameters meet specified conditions. When $d = \lambda/2$, broad beams can be obtained in the cases of $dp = 0°$, $dp = 30°$, and $dp = 60°$. When $d = \lambda/8$, broad beams can be obtained in the cases of $dp = 0°$ and $dp = 30°$. From Fig. 2, we can also see that the beamwidth in the $\varphi = 45°/-135°$ plane and the gain fluctuation of the pattern in xy plane intuitively show the broad-beam performance of each case.

To discuss the effect of distance d on the pattern, the half-power beamwidths (HPBW) in the $\varphi = 45°/-135°$ plane at 2.4 GHz corresponding to different d are shown in Fig. 3. In all of the cases, distance d_2 is fixed at $\lambda/2$. From Fig. 3, we can see that good broad-beam performances can be obtained when the phase difference dp is within 30° and the distance d between $\lambda/8$ and $\lambda/2$. Similarly, the HPBW in the $\varphi = 45°/-135°$ plane corresponding to the different distance d_2 is shown in Fig. 4. From Fig. 4, we can see that good broad beams can be obtained when phase difference dp is within

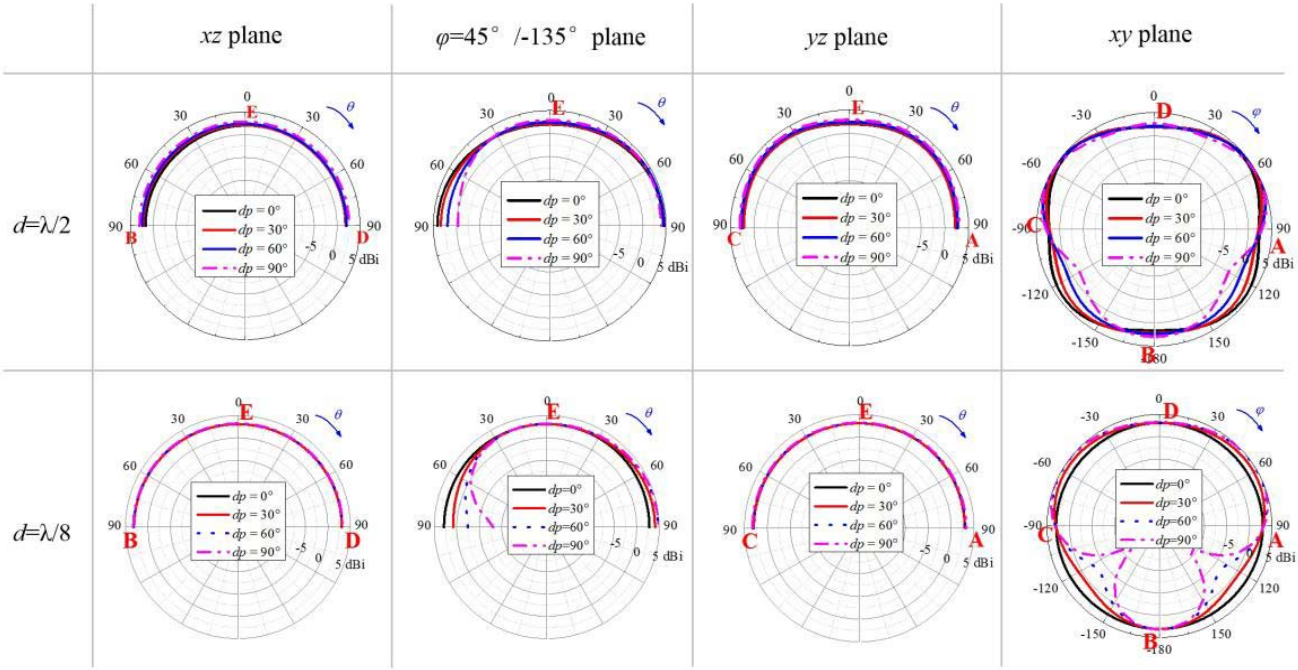

Figure 2. The effect of dp on the radiation patterns at 2.4 GHz of the TC model.

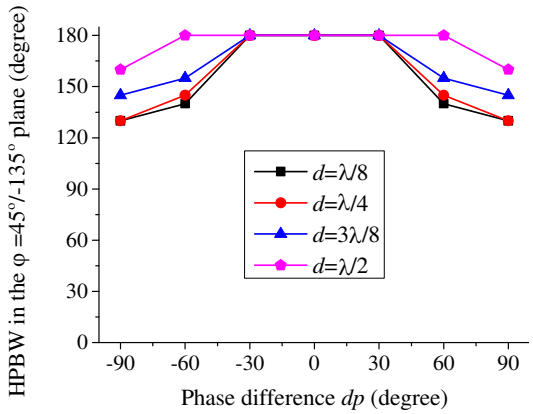

Figure 3. HPBW in the $\varphi = 45°/-135°$ plane at 2.4 GHz corresponding to the different distance d.

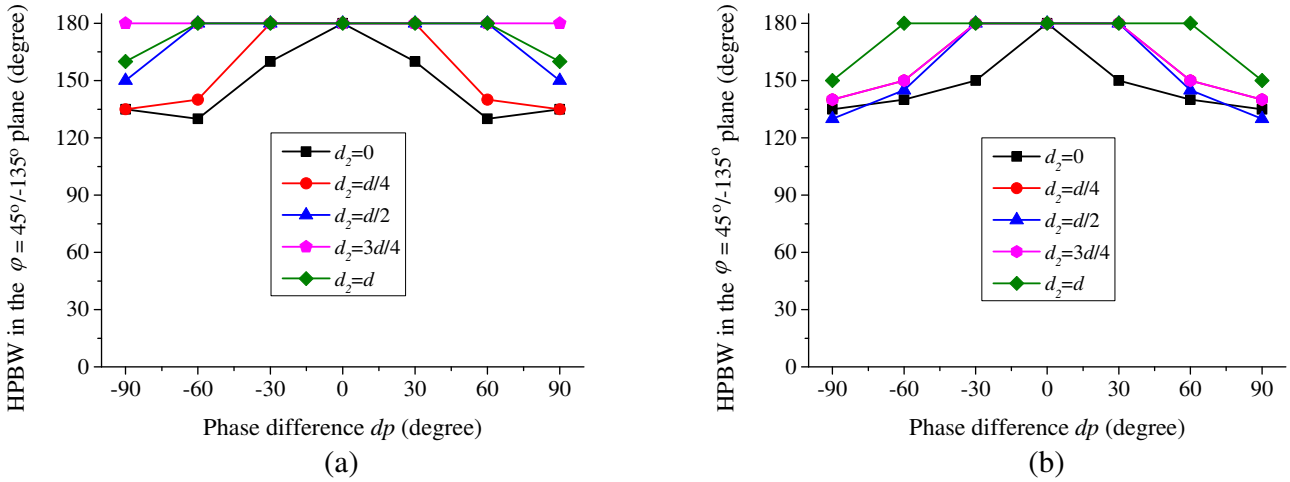

Figure 4. HPBW in the $\varphi = 45°/-135°$ plane at 2.4 GHz corresponding to the different distance d_2, when (a) $d = \lambda/2$ and (b) $d = \lambda/4$.

30° and distance d_2 between $d/4$ and d. In the case of $d_2 = 0$, good broad beams can only be obtained when Dipole 1 and Dipole 2 have equal phase.

From the above discussions, we can make a conclusion that if C1 and C2 of the TC model have an equal initial excited phase, a good broad beam can be obtained when d and d_2 change in a relatively wide range, which provides a great design freedom for the antenna structure.

Next, a three-element antenna will be designed under a special circumstance of Eqn. (3), $d = \lambda/2$ and $A_2 = 2A_1$, when C1 and C2 of the TC model have an equal initial excited phase. In the design, the distance between Elements 1 and 3, noted as d, is set as $\lambda/2$ to meet the special circumstance of $A_2 = 2A_1$ according to Eqn. (3), and an inverted-T-shape feeding line is designed to provide three elements with equal phases.

3. BROAD-BEAM ON-BOARD ANTENNA BASED ON THE THREE-CURRENT MODEL

3.1. Generation of Directed Equivalent Magnetic Current

Two kinds of antennas can be designed based on the proposed TC model, one of which is electric currents parallel to a magnetic wall, and the other is magnetic currents parallel to an electric wall, i.e., an ideal metal ground. Now, we verify the TC model with directed equivalent magnetic currents.

A microstrip patch with three edges grounded can be used to generate equivalent magnetic current [25]. Using semi-closed microstrip cavity, a magnetic-current antenna is designed, as shown in Fig. 5. Color brown represents copper material, and color aquamarine represents dielectric substrate. The dielectric substrate has a thickness of 4 mm and relative dielectric constant of 2.65. A copper patch with three grounded edges is printed on the substrate and fed from the backside. The feeding point is located at the centre of the copper patch along the x-axis. The CST Microwave Studio is used to simulate and optimize all the antennas in this paper. The optimum dimensions of the magnetic-current antenna are shown in Fig. 5.

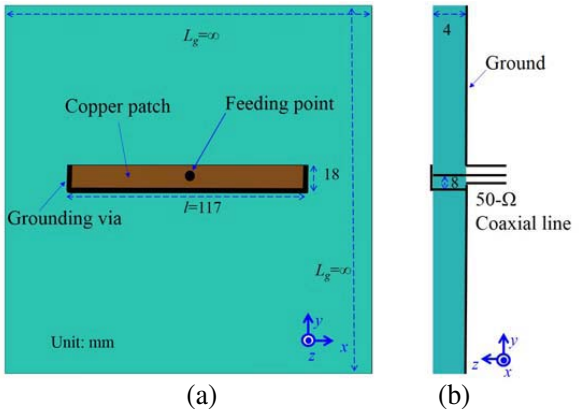

Figure 5. Geometry of the magnetic-current antenna: (a) front view and (b) side view.

The proposed antenna has only one edge opened and the other three edges shorted. The long shorted edge can make sure that the proposed antenna provides a single magnetic element, which produces vertical electric field. Radiation is contributed only from the open aperture, which can be considered as a "magnetic current antenna". As a comparison, the opposite two edges of general microstrip patch antennas can be considered as two magnetic elements. The magnetic field distribution of the magnetic-current antenna is shown in Fig. 6. The directed equivalent magnetic current along the open edge has been marked in the figure.

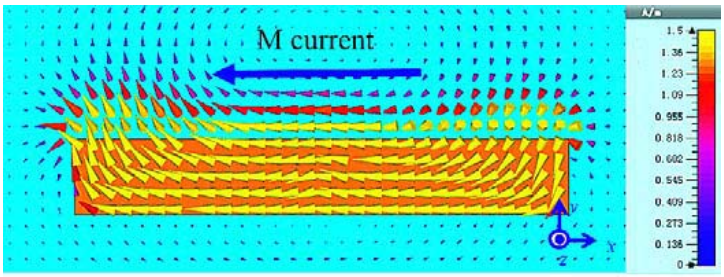

Figure 6. Magnetic field distribution of the magnetic-current antenna.

The reflection coefficients and far-field patterns at 2.4 GHz of the magnetic-current antenna corresponding to different values of the patch length l is shown in Fig. 7. We can see that the resonant frequency and 3-dB beamwidth in the xz plane decrease with increasing l. It is notable that when l changes from 78 mm to 156 mm (double), the resonant frequency only changes from 2.62 GHz to 2.3 GHz (0.88 times instead of 0.5 times), because the feeding point is located at the centre of the copper patch along the x-axis and because the amplitude of equivalent magnetic current becomes weak away from the feeding point. This is different from electric current antennas. For these situations, the 3-dB beams of the magnetic-current antenna can cover from the broadside direction to end-fire direction in the yz plane and can only cover the broadside direction in the xz plane, which agrees well with the radiation performance of the single magnetic dipole.

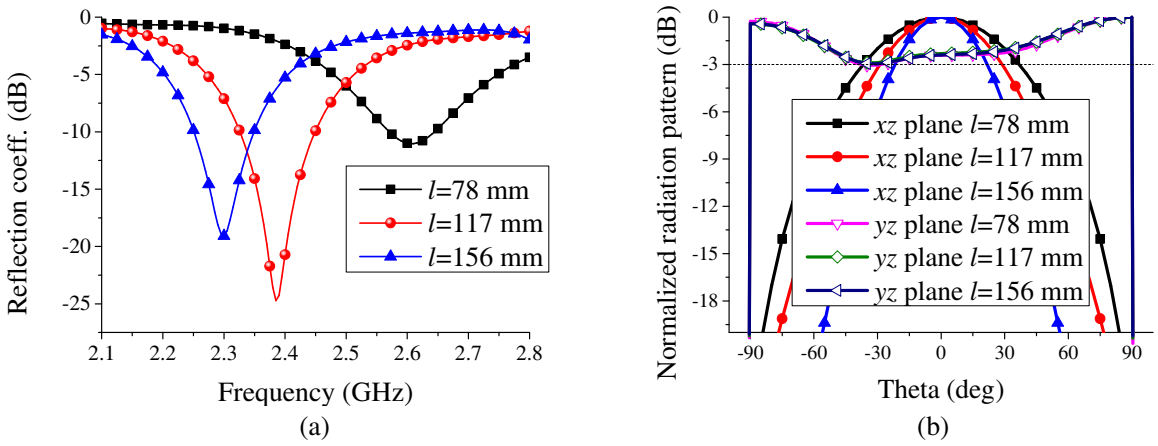

Figure 7. (a) Reflection coefficients and (b) radiation patterns at 2.4 GHz of the magnetic current antenna.

3.2. Broad-Beam On-Board Antenna with Three Elements

Now, we construct a three-element antenna based on the TC model with three directed equivalent magnetic currents. We take four steps to design the three-element antenna as shown in Fig. 8. Step 1, a magnetic-current antenna is designed. Step 2, three antennas designed in Step 1 are combined according to the three current model. Step 3, a feeding network is designed. Step 4, the three elements in Step 2 and the feeding network in Step 3 are combined, and the final antenna is achieved to be fabricated.

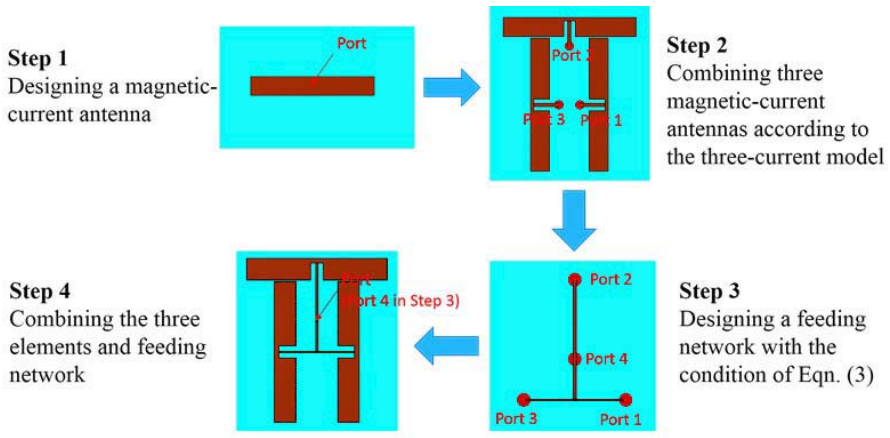

Figure 8. The processes to design the three-element antenna.

The geometry of the three-element antenna is shown in Fig. 9. According to Eqn. (3), when the distance between Elements 1 and 2 is given, the amplitude of exciting signal of each element can be determined. The distance between Elements 1 and 3 is set as $d = \lambda/2$, therefore $A_2 = 2A_1$, where λ is the free-space wavelength corresponding to 2.4 GHz; A_1 and A_2 are exciting amplitudes of Elements 1 and 2. The inverted-T-shaped feeding network can provide three elements with equal phases and provide Element 2 with an amplitude double of that for Elements 1 and 3 by adjusting the line widths and feeding position. The equivalent magnetic currents of Elements 1 and 3 have opposite directions because of the structure.

One of the main differences between the proposed TC model and the implementation in prototype is the coupling among three elements. To show the port-coupling, the active S parameters of the three elements in Step 2 are shown in Fig. 10(a). The ports of Elements 1, 2, and 3 are noted as Ports 1, 2, and 3, respectively. From this figure, we can see that the insertion losses between every two ports are

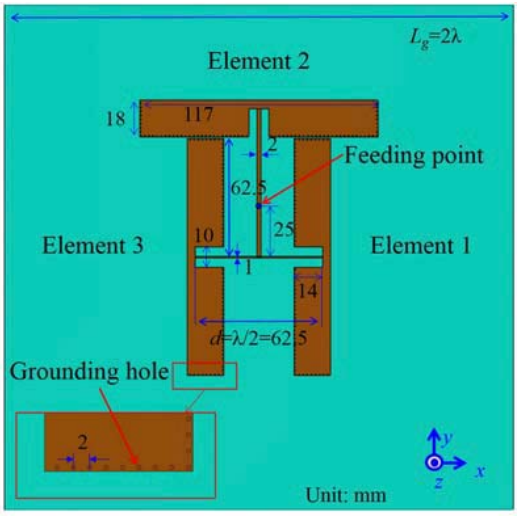

Figure 9. Geometry of the three-element antenna.

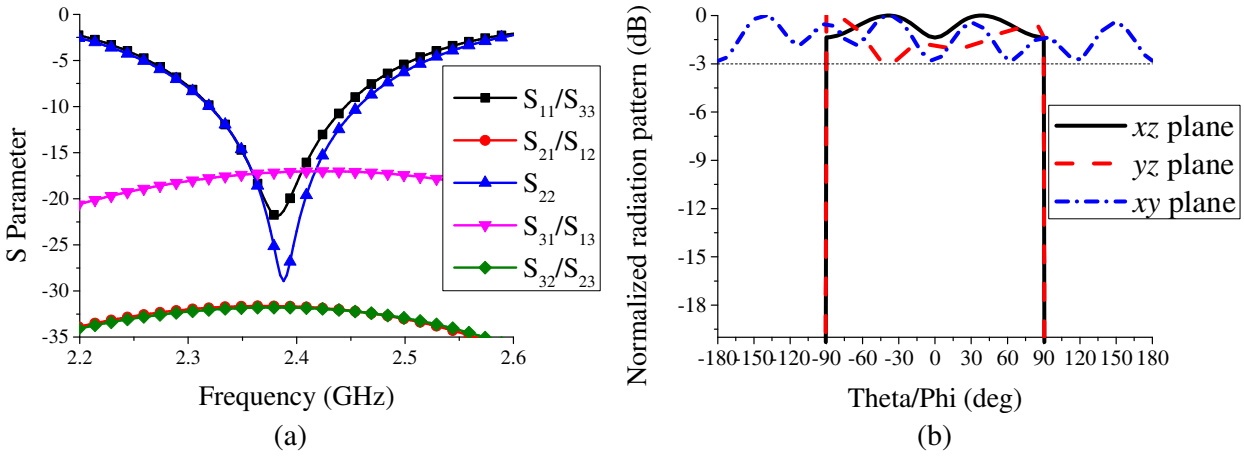

Figure 10. (a) The active S parameters of the three elements. (b) Radiation patterns at 2.4 GHz of the three-element antenna with an infinite ground.

all more than 15 dB. The weak coupling allows the proposed antenna to agree with the TC model.

To show the broad-beam performance, the three elements in Step 2 without inverted-T-shaped feeding network are fed with equal phases, and Element 2 is fed with an amplitude double of Elements 1 and 3. When side length L_g of the ground is infinite, the far-field radiation patterns at 2.4 GHz of the three-element antenna are shown in Fig. 10(b). The 3-dB beamwidths in the xz plane and yz plane are all 180°, and the radiation pattern in the xy plane has a gain fluctuation less than 3 dB. This verification example shows that the TC model is available for practical antenna design.

After Step 2, the positions of three elements are fixed, and only three parameters, two line widths and a feeding position, can be adjusted in our inverted-T-shaped feeding network. Among the three parameters which can be adjusted, two line widths mainly affect the magnitudes, and the feeding position mainly affects the phases. Considering that the relation in Eqn. (3) is from electric field, the magnitudes (proportional to voltage) and phases of the S parameters of the feeding network in Step 3 are shown in Fig. 11. From Fig. 11, we can see that the proposed feeding network can provide three elements with similar phases and provide Element 2 with an amplitude about double of that for Elements 1 and 3 at around 2.4 GHz.

The magnetic field distribution of the three-element antenna with inverted-T-shaped feeding

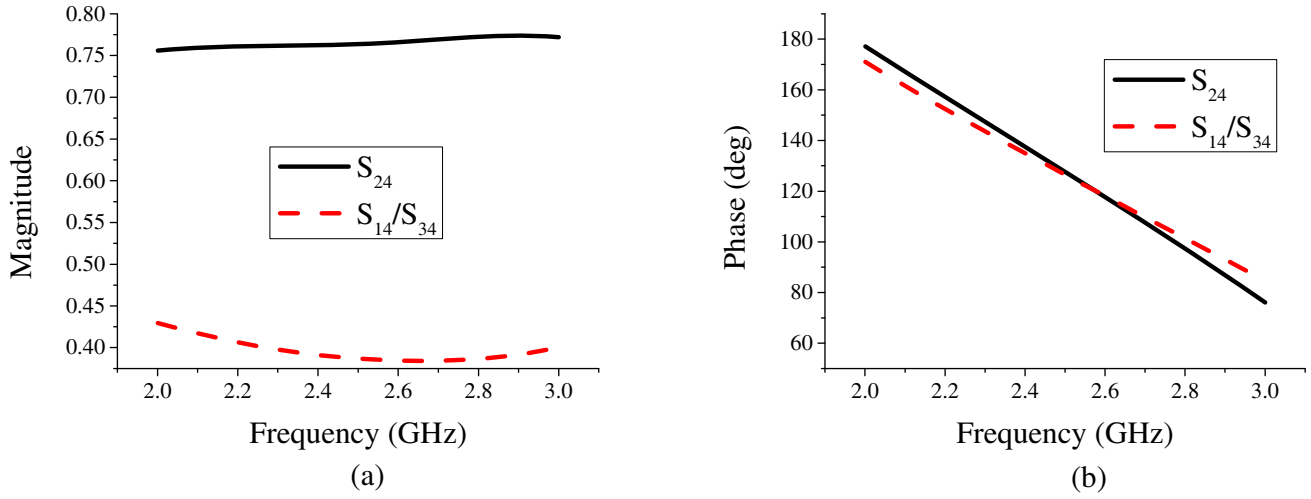

Figure 11. (a) The magnitudes and (b) phases of the S parameters of the inverted-T-shape feeding network.

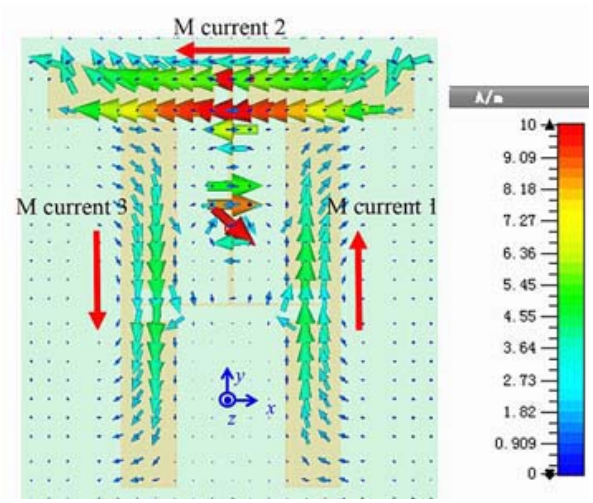

Figure 12. Magnetic field distribution of the three-element antenna.

network is shown in Fig. 12, and the directed equivalent magnetic currents have been marked in the figure. The figure shows that the equivalent magnetic currents satisfy the TC model.

A prototype of the proposed antenna with $L_g = 2\lambda$ is fabricated, and two photographs are shown in Fig. 13. The simulated and measured reflection coefficients of the proposed antenna with inverted-T-shaped feeding network are shown in Fig. 14. The simulated band with S_{11} below -10 dB is between 2.33 GHz and 2.44 GHz, and the measured one is between 2.34 GHz and 2.47 GHz. The measured resonant frequency has moved a little toward high frequency because of the machining error, which includes the parameters error of practical substrate, etching error of copper layer, impedance error of SMA connector and soldering error.

The far-field radiation pattern is measured in a microwave anechoic chamber. The simulated and measured radiation patterns of the proposed antenna are shown in Fig. 15. In these figures, FN represents the inverted-T-shaped feeding network. To analyze the effect of feeding network, the simulated results include patterns of the proposed antenna with and without inverted-T-shaped feeding network. From the two kinds of simulated patterns, in the xz plane, Elements 1 and 3 result in two split-lobes and the radiation of feeding line increases the amplitude in the broadside direction. When $L_g = 2\lambda$, the measured 3-dB beamwidths in the xz plane and yz plane are 141° and 148°, respectively.

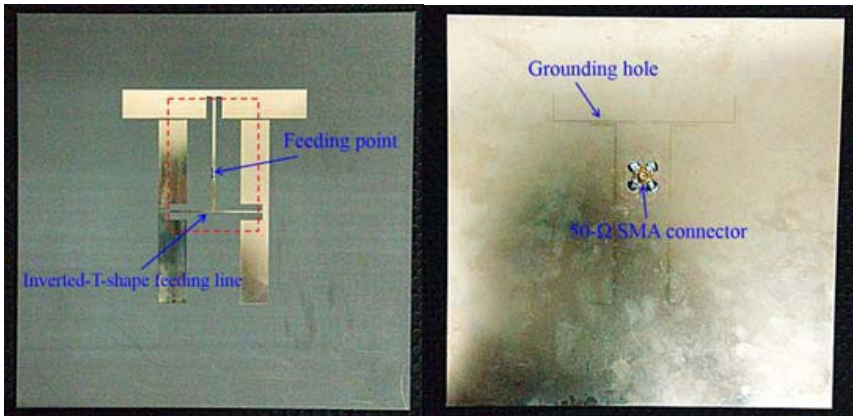

Figure 13. Photographs of the fabricated three-element antenna: (a) top side and (b) bottom side.

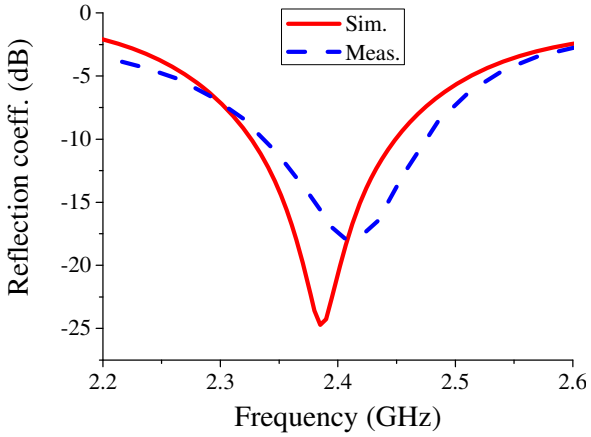

Figure 14. Simulated and measured reflection coefficients of the proposed three-element antenna.

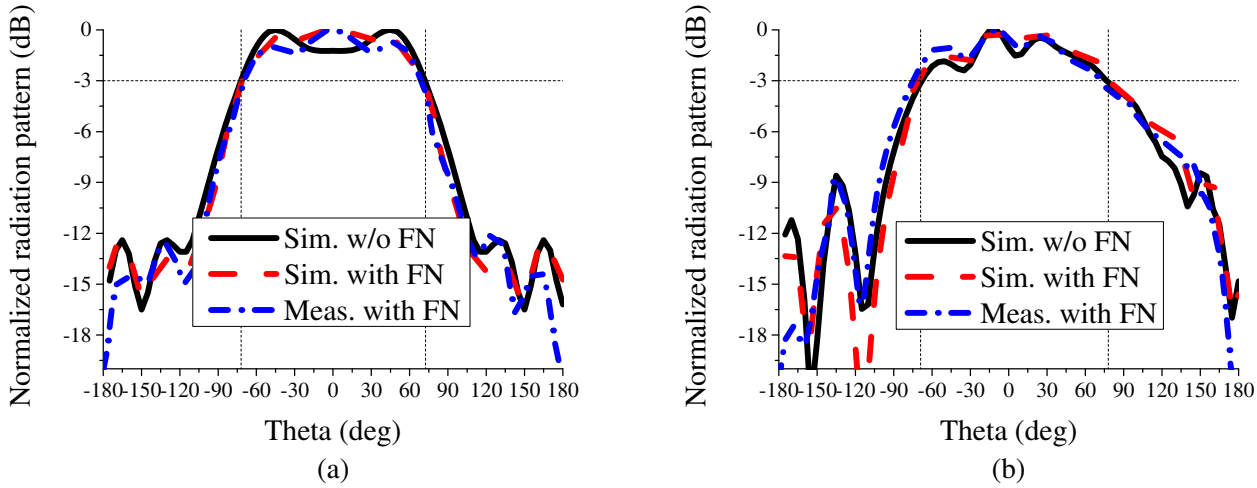

Figure 15. Simulated and measured (a) xz plane patterns and (b) yz plane patterns at 2.4 GHz of the three-element antenna.

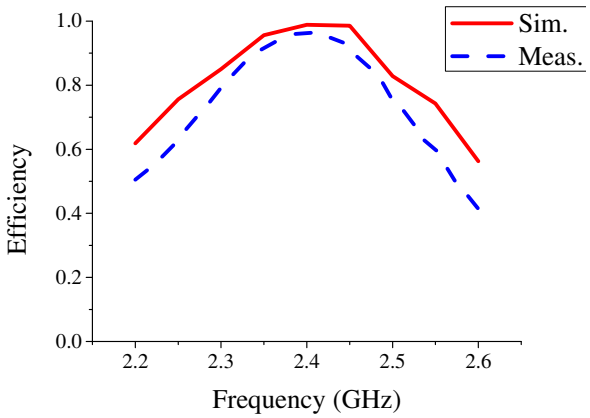

Figure 16. Simulated and measured efficiencies of the three-element antenna.

The simulated and measured efficiencies of the proposed antenna are shown in Fig. 16. The simulated and measured efficiencies are both more than 80% in the operation frequency band. The measured efficiency is a little lower than the simulated one because of the losses of metal and substrate.

The above discussions show that the ground size of the proposed antenna has an obvious effect on the broad coverage performance. The ground of the on-board antenna is practically limited to the dimension of the carrier. In vehicle-mounted applications, the roof panel is approximately $1.5 \times 1.5\,\mathrm{m}^2$, approximately $12\lambda \times 12\lambda$, and the dimension of a car is approximately $1.8 \times 4.8\,\mathrm{m}^2$. An example of the proposed antenna placed on the roof panel of a car is shown in Fig. 17(a).

The radiation patterns in the xz plane and yz plane at 2.4 GHz of the proposed antenna placed on the roof panel of a car are shown in Fig. 17(b). Some fluctuations occur on the radiation patterns because of the complex scattering of the car. The 3-dB beamwidths of pattern envelopes in the xz plane and yz plane are respectively 150° and 180°. The 5-dB beamwidth of pattern envelope in the xz plane is about 180°. The beamwidth in the yz plane is wider than that in the xz plane because the size of the car along y axis is longer than that along x axis. This example shows that a broad beam can be obtained when the proposed antenna has a carrier.

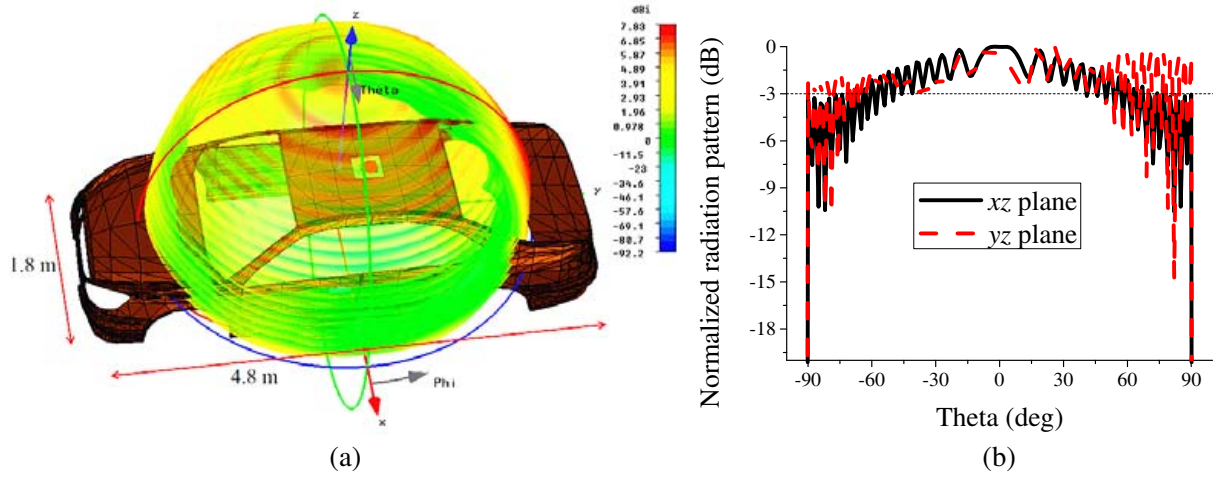

Figure 17. (a) The three-element antenna placed on the roof panel of a car and (b) its simulated patterns at 2.4 GHz.

From Fig. 15(b) and Fig. 17(b), we can see that the imbalance created by Element 2 results in a tilted beam in the yz plane. In Fig. 17(b), although there is a pattern tilting phenomenon, the 3-dB beamwidth of pattern envelope in the yz plane can reach 180°. In other words, when the ground size

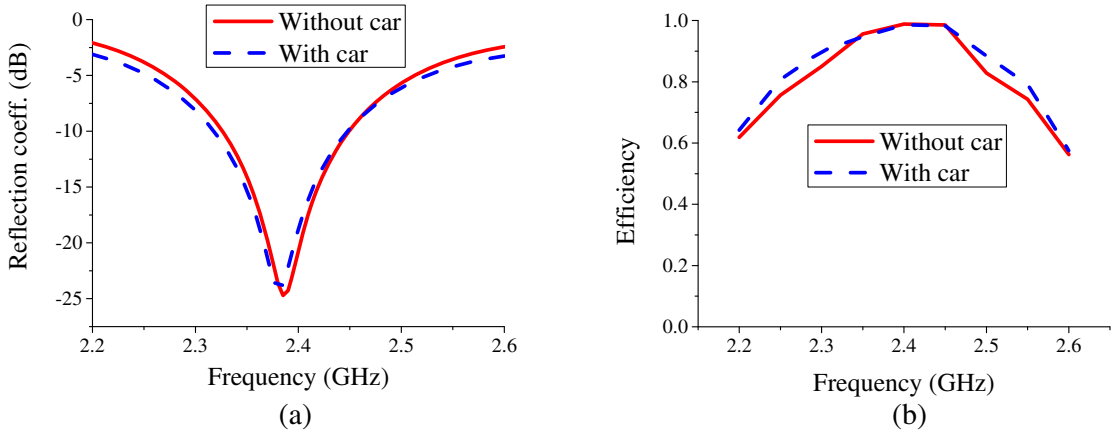

Figure 18. (a) Simulated reflection coefficients and (b) efficiencies of the three-element antenna with and without a car.

is large enough, the tilting phenomenon has a sufferable effect on broad beam. Fortunately, antennas based on the TC model that we proposed are suitable for the on-board situations with a large ground because this model can adequately show the broad-beam performance when the ground is large enough. Therefore, the effect of pattern tilting is acceptable to the broad-beam performance.

In addition, the simulated reflection coefficients and efficiencies of the three-element antenna with and without a car are shown in Fig. 18. Because the radiation of the proposed antenna on the roof of a car is mainly directed to the upper half-space, the car body has little effects on the impedance matching and radiation efficiency.

4. CONCLUSION

In this paper, a three-current model is proposed to guide the design of on-board antennas with a broad beam. A design example of on-board three-element antenna shows that a broad beam can be obtained based on this model. The proposed antenna can be used in wireless communication systems. In addition, the proposed three-element antenna is one of the schemes to realize the TC model, and there may be some other compact structures based on the proposed model which are valuable to study.

ACKNOWLEDGMENT

This work was supported by the National Natural Science Foundation of China (Grant Nos. 61331007, 61361166008,and 61401065), the Specialized Research Fund for the Doctoral Program of Higher Education of China (Grant No. 20120185130001), and EHF key Laboratory of Fundamental Science Project A030100238011710003.

REFERENCES

1. Chen, C., Z. Li, L. Liu, J. Xu, P. Ning, B. Xu, X. Chen, and C. Gu, "A circularly-polarized metasurfaced dipole antenna with wide axial-ratio beamwidth and RCS reduction functions," *Progress In Electromagnetics Research*, Vol. 154, 79–85, 2015.
2. Wu, H. and T. Zwick, "Octave division motion compensation algorithm for near-range wide-beam SAR applications," *Progress In Electromagnetics Research*, Vol. 144, 115–122, 2014.
3. Khalifa, I. and R. G. Vaughan, "Geometric design and comparison of multifaceted antenna arrays for hemispherical coverage," *IEEE Trans. Antennas Propag.*, Vol. 57, No. 9, 2608–2614, 2009.
4. Panduro, M. A. and C. del Rio Bocio, "Design of beam-forming networks for scannable multi-beam antenna arrays using corps," *Progress In Electromagnetics Research*, Vol. 84, 173–188, 2008.

5. Wang, R., B.-Z. Wang, X. Ding, and X.-S. Yang, "Planar phased array with wide-angle scanning performance based on image theory," *IEEE Trans. Antennas Propag.*, Vol. 63, No. 9, 3908–3917, 2015.
6. Ta, S. X. and I. Park, "Crossed dipole loaded with magneto-electric dipole for wideband and wide-beam circularly polarized radiation," *IEEE Antennas Wireless Propag. Lett.*, Vol. 14, 358–361, 2015.
7. Choi, E., J. W. Lee, and T. Lee, "Modified S-band satellite antenna with isoflux pattern and circularly polarized wide beamwidth," *IEEE Antennas Wireless Propag. Lett.*, Vol. 12, 1319–1322, 2013.
8. Wang, P., G. Wen, J. Li, Y. Huang, L. Yang, and Q. Zhang "Wideband circularly polarized UHF RFID reader antenna with high gain and wide axial ratio beamwidths," *Progress In Electromagnetics Research*, Vol. 129, 365–381, 2012.
9. Valavan, S. E., D. Tran, A. G. Yarovoy, and A. G. Roederer, "Planar dual-band wide-scan phased array in x-band," *IEEE Trans. Antennas Propag.*, Vol. 62, No. 10, 5370–5375, 2014.
10. Valavan, S. E., D. Tran, A. G. Yarovoy, and A. G. Roederer, "Dual-band wide-angle scanning planar phased array in X/Ku-bands," *IEEE Trans. Antennas Propag.*, Vol. 62, No. 5, 2514–2521, 2014.
11. Altshuler, E. E., "A monopole antenna loaded with a modified folded dipole," *IEEE Trans. Antennas Propag.*, Vol. 41, No. 7, 871–876, 1993.
12. Altshuler, E. E. and D. S. Linden, "Design of a loaded monopole having hemispherical coverage using a genetic algorithm," *IEEE Trans. Antennas Propag.*, Vol. 45, No. 1, 1–4, 1997.
13. Nishizawa, K., H. Miyashita, S. Makino, and K. Sawaya, "Broad beamwidth and cross polarization free dipole antennas with reactive loaded monopoles," *IEEE Trans. Antennas Propag.*, Vol. 55, No. 5, 1230–1238, 2007.
14. Wang, R., B.-Z. Wang, X. Ding, Z.-S. Gong, Y. Yang, and Y.-Q. Wen, "A wide-angle scanning array based on image theory and time reversal synthesis method," *2015 IEEE International Symposium on Antennas and Propagation*, 2495–2496, 2015.
15. Wu, C., L. Han, F. Yang, L. Wang, and P. Yang, "Broad beamwidth circular polarisation antenna: Microstrip-monopole antenna," *Electron. Lett.*, Vol. 48, No. 19, 1176–1178, 2012.
16. Prinsloo, D. S., R. Maaskant, M. V. Ivashina, and P. Meyer, "Mixed-mode sensitivity analysis of a combined differential and common mode active receiving antenna providing near-hemispherical field-of-view coverage," *IEEE Trans. Antennas Propag.*, Vol. 62, No. 8, 3951–3961, 2014.
17. Alù, A. and N. Engheta, "Cloaking a sensor," *Phys. Rev. Lett.*, Vol. 102, No. 23, 233901, 2009.
18. Greenleaf, A., Y. Kurylev, M. Lassas, and G. Uhlmann, "Cloaking a sensor via transformation optics," *Phys. Rev. E*, Vol. 83, 211–222, 2011.
19. Valagiannopoulos, C. A. and N. L. Tsitsas, "Integral equation analysis of a low-profile receiving planar microstrip antenna with a cloaking superstrate," *Radio Sci.*, Vol. 47, No. 2, 49-57, 2012.
20. Valagiannopoulos, C. A., N. L. Tsitsas, and A. H. Sihvola, "Hiding a bump on a PEC plane by using an isotropic lossless dielectric layer," *IEEE Trans. Antennas Propag.*, Vol. 62, No. 11 5706–5714, 2014.
21. Valagiannopoulos, C. A., P. Alitalo, and S. A. Tretyakov, "On the minimal scattering response of PEC cylinders in a dielectric cloak," *IEEE Antennas Wireless Propag. Lett.*, Vol. 13, 403–406, 2014.
22. Alitalo, P., "Electromagnetic cloaking of cylindrical objects by multilayer or uniform dielectric claddings," *Phys. Rev. B*, Vol. 85, No. 85, 1092–1097, 2012.
23. Kundtz, N., D. Gaultney, and D. R. Smith, "Scattering cross-section of a transformation optics-based metamaterial cloak," *New J. Phys.*, Vol. 12, No. 16, 043039, 2010.
24. Balanis, C. A., *Antenna Theory, Analysis and Design*, 2nd Edition, Wiley, New York, USA, 1997.
25. Liu, J. and Q. Xue, "Microstrip magnetic dipole Yagi array antenna with endfire radiation and vertical polarization," *IEEE Trans. Antennas Propag.*, Vol. 61, No. 3, 1140–1147, 2013.